The Cryosphere Discuss., 7, 841–871, 2013
www.the-cryosphere-discuss.net/7/841/2013/
doi:10.5194/tcd-7-841-2013

The Cryosphere Discussions
Open Access

Cascading water underneath Wilkes Land, East Antarctic Ice Sheet, observed using altimetry and digital elevation models

T. Flament, E. Berthier, and F. Rémy

CNRS, LEGOS, UMR5566 CNRS-CNES-IRD-Université de Toulouse III, 14 Avenue Edouard Belin, 31400 Toulouse, France

Received: 6 February 2013 – Accepted: 19 February 2013 – Published: 5 March 2013

Correspondence to: T. Flament (thomas.flament@legos.obs-mip.fr)

Published by Copernicus Publications on behalf of the European Geosciences Union.

Abstract

We describe a major subglacial lake drainage close to the ice divide in Wilkes Land, East Antarctica, and the subsequent cascading of water underneath the ice sheet toward the coast. To analyze the event, we combined altimetry data from several sources and bedrock data. We estimated the total volume of water that drained from Lake $Cook_{E2}$ by differencing digital elevation models (DEM) derived from ASTER and SPOT5 stereo-imagery. With $5.2 \pm 0.5\,km^3$, this is the largest single subglacial drainage event reported so far in Antarctica. Elevation differences between ICESat laser altimetry and the SPOT5 DEM indicate that the discharge lasted approximately 2 yr. A 13-m uplift of the surface, corresponding to a refilling of about $0.64 \pm 0.32\,km^3$, was observed between the end of the discharge in October 2008 and February 2012. Using Envisat radar altimetry, with its high 35-day temporal resolution, we monitored the subsequent filling and drainage of connected subglacial lakes located downstream. In particular, a transient temporal signal can be detected within the theoretical 500-km long flow paths computed with the BEDMAP2 data set. The volume of water traveling in this wave is in agreement with the volume that drained from Lake $Cook_{E2}$. These observations contribute to a better understanding of the water transport beneath the East Antarctic ice sheet.

1 Introduction

The presence of water beneath the Antarctic ice sheet has been known for several decades. A well-known example of a subglacial lake is Lake Vostok, a reservoir containing about $5000\,km^3$ of liquid water beneath approximately 4000 m of ice, in East Antarctica (Siegert, 2005). It might seem surprising that liquid water can exist under the ice of the coldest continent on Earth. A thick layer of ice can provide sufficient insulation for the small geothermal and ice-deformation heat fluxes to melt the ice sheet at its base and keep the water liquid (Siegert and Dowdeswell, 1996). This mechanism

TCD
7, 841–871, 2013

explains the presence of lakes under the thick central plateau of the ice sheet. In other places, under fast flowing ice streams, the energy for melting water is yielded by friction on the bed (Joughin et al., 2004).

Recent studies used repeated satellite measurements and reported surface elevation changes linked to the temporal evolution of subglacial lake volume (e.g. Wingham et al., 2006; Fricker et al., 2007; Gray et al., 2005). Water flowing below the ice sheet induces movements of the surface as ice is lifted or lowered by floatation when lakes fill in or drain (Clarke, 2006). These discoveries led to a better general understanding of the dynamic nature of subglacial hydrological systems (Fricker and Scambos, 2009). The further our knowledge of these systems goes, the more we realize their role on ice sheet dynamics. This impact of subglacial water on ice sheet dynamics is still being investigated (e.g. Bell et al., 2007; Stearns et al., 2008; Schoof, 2010) and it is not taken explicitly into account in any large scale model yet.

Smith et al. (2009) provided the first inventory of active subglacial lakes in Antarctica from repeat ICESat laser altimetry. In particular, they observed a strong drawdown of the ice surface in Wilkes Land (−72.803° N, 155.786° E, upstream from the Cook Ice Shelf) and attributed it to the drainage of a lake they named Cook_{E2}. Along several kilometers on two crossing ICESat tracks, the surface lowered by up to 65 m between November 2006 and March 2008. They estimated that 2.7 km^3 of water was discharged during this event, the largest drainage event reported so far in Antarctica. Here, we revisit this exceptional event in more detail using radar (Envisat) and laser (ICESat) along-track altimetry and by differencing multi-temporal digital elevation models (SPOT5 and ASTER). We take advantage of the good spatial/temporal coverage from multiple instruments to (i) recalculate the total volume of water that drained from the Lake Cook_{E2}, (ii) document the changes that this lake has undergone since the end of the drainage and (iii) study the downstream consequences of this discharge.

TCD
7, 841–871, 2013

2 Data and method

2.1 Envisat measurements

Elevation measurements from the Envisat radar altimeter (RA-2) during 85 repeat cycles from September 2002 till October 2010 are used. The along-track processing used here has been presented in detail by Flament and Rémy (2012). It is similar to other least-square processing techniques presented elsewhere for ICESat data (Smith et al., 2009; Sørensen et al., 2011; Moholdt et al., 2010), adapted to the characteristics of radar altimetry.

Measurements are collected in sections of 1 km along track and processed by a least square fit. Corrections for local topography (slope and curvature) and echo shape (backscatter, leading edge width and trailing edge slope) are applied. This processing provides a spatially and temporally dense data set, suitable for the study of short-lived and small scale phenomena such as subglacial lake drainages. Elevation time series are also derived from the output of the fit; at time t, the elevation is given by:

$$H(t) = \varepsilon(t) + \mathrm{d}h/\mathrm{d}t \cdot (t - t_0)$$

where $\varepsilon(t)$ is the residual at time t, $\mathrm{d}h/\mathrm{d}t$ is the linear elevation trend and t_0 is an arbitrary reference time. Here, we tune t_0 to obtain $H(t) = 0$ when $t = 2006.85$ (the choice of this date is justified in Sect. 5.2).

Noise in the processed series is computed as the standard deviation of the difference between the time series and a smoothed time series. In other words, the higher frequencies are considered as noise and removed. This noise level is very dependent on the kilometer-scale topography and can vary from under one decimeter in a flat and horizontal area to several meters over rugged terrain. In the following, time series are considered of acceptable quality if this noise is below 1 m.

TCD
7, 841–871, 2013

2.2 ICESat measurements

ICESat measurements are taken from release 31 available from the NSIDC (http://nsidc.org/data/icesat/index.html) and span campaigns 2A to 2F, from October 2003 to October 2009. The last complete campaign was 2E (Spring 2009). ICESat coordinates were first converted from the TOPEX/Poseidon to the WGS-84 ellipsoid. ICESat ellipsoidal heights were then converted to altitudes using the EGM96 geoid, EGM96 being the reference for the SPOT5 and ASTER DEMs (see below).

2.3 Digital elevation models from stereo-imagery

Digital Elevation Models (DEM) of the area surrounding Lake $Cook_{E2}$ were constructed from stereo-pairs of optical images acquired by two space-borne sensors: ASTER (Toutin, 2008) and SPOT5-HRS (Korona et al., 2009). Comparing multi-temporal DEMs is useful for measuring elevation changes in mountainous areas (e.g. Gardelle et al., 2012) or at the steeper ice sheet margins (e.g. Howat et al., 2007), where other altimetry techniques do not perform as well or lack sufficient across-track coverage. DEM differencing has only been used once before to characterize the drainage of a subglacial lake, in response to the rapid thinning of Crane Glacier in the Antarctic Peninsula (Scambos et al., 2011). However, DEMs from optical imagery are still regarded as being of limited use for the study of the central part of ice sheets because of the lack of identifiable features on their surface (e.g. Bindschadler et al., 2011).

Here, we take advantage of some recent improvements achieved by the French mapping agency (IGN, Institut Géographique National) in the processing of stereo-pairs on low contrast areas to derive a nearly complete DEM of the Lake $Cook_{E2}$ area from SPOT5-HRS imagery acquired on 9 February 2012, about 3 years after the drainage ended. Those improvements consisted in (i) reducing the size of the final correlation window to match small scale variations in radiometry present in the two images of the stereo-pair; and (ii) accepting DEM pixels with a correlation score (CS, ranging from 0 to 100) lower (CS > 30) than for the standard IGN algorithm that retained pixels with

TCD
7, 841–871, 2013

CS > 50. Those modifications improved the DEM coverage. Importantly, it was verified using ICESat data that the newly-retained DEM pixels had the same level of accuracy as the pixels retained in the standard algorithm. By means of an appropriate gain setting during the image acquisition and the above-mentioned improved set of correlation parameters, gaps in the SPOT5 DEM only cover 1 % of the study area (versus 51 % using the former processing). The surface topography prior to the drainage start is derived from an ASTER stereo-pair acquired on 26 January 2006. The ASTER DEM and the corresponding correlation mask were calculated using PCI Geomatica 10.1 (Toutin, 2008). Unreliable pixels, covering 60 % of the area of interest, were masked in the ASTER DEM.

Vertical biases in the pre- and post- drainage DEMs were estimated and corrected using ICESat. We extracted the ASTER and SPOT5 DEM elevations for each ICESat footprint using bilinear interpolation. Compared with all the data from laser period 3E (mean date: 12 March 2006), a vertical bias of −7.2 m (standard deviation, SD = 11.7 m, N = 1039) was derived and corrected for the 26 January 2006 ASTER DEM. The SPOT5 DEM was also compared to laser period 3E but only outside the lake area. A mean bias of 11.6 m (SD = 2.1 m, N = 8246) was found. There was a tilt in the SPOT 5 DEM in the North/South direction which we also corrected by fitting a plane to the elevation differences with ICESat. After correction of this tilt, the standard deviation of the elevation difference is reduced to 1.6 m (laser period 3E, N = 8246). This vertically-adjusted SPOT5 DEM was then compared to ICESat data from other laser periods outside of the lake area. The absolute mean difference was always lower than 0.5 m, indicating the stability of the region surrounding the lake. The standard deviations of the elevation differences were similar for all laser periods (range: 1.50 m to 1.67 m).

Reliable values in the ASTER DEM covered only 40 % of our area of interest. To obtain a complete pre-event topography, the altitude contour lines from the vertically-adjusted SPOT5 DEM (generated with an altitude step of 5 m) were used away from the lake and extended in the $Cook_{E2}$ area using similar 5-m altitude contour lines generated from the vertically-adjusted ASTER DEM. We extracted from pre-drainage ICESat

TCD
7, 841–871, 2013

data the locations where ICESat tracks had the same elevation as the DEM contours. ASTER contour lines were then extended manually to pass through ICESat points at the same elevation. This pre-event altitude contour map was then gridded to obtain a complete pre-event DEM. The pre- and post-event DEMs are then differentiated to obtain the map of elevation differences and to infer the total volume loss during the drainage.

3 Drainage of Lake Cook$_{E2}$

DEM differencing, differences between ICESat and the SPOT5 DEM are used to analyze the drainage of Cook$_{E2}$ and re-estimate the total volume of water discharged.

Luckily, ICESat tracks cross almost at the location where the surface lowering is greatest (Fig. 1) and thus provide a temporally well-resolved view of the drainage (Fig. 2). In the center of the main lake, the total surface lowering reached 70 m between laser campaign 3G (November 2006) and 3K (March 2008). The map of elevation differences also shows that, in addition to this main lake, a secondary lake drained simultaneously leading to a maximum surface lowering of 30 m. Since March 2009, a surface uplift of 13 m is observed in the central part of the depression.

Following Smith et al. (2009), we assumed that the volume changes measured at the ice sheet surface equal the volume of water that drained from the lake. The total drainage is thus the product of the "lake area" by the mean elevation difference within this area. The lake area is defined as all the pixels where the surface lowering is greater than 3 m. The sensitivity of our result to this arbitrary choice is tested by estimating the lake discharge when the threshold for minimum surface lowering is set to 1.5 m and 4.5 m. With a threshold at 3 m, the lake area is 219 km^2 and the mean surface lowering 20.6 m, leading to a lake discharge of 4.52 km^3 of water. This volume varies by 0.1 km^3 (referred to as the "lake-area" error) when the upper (1.5 m) and lower (4.5 m) limits for the surface lowering are used to determine the extent of the lake area (Fig. 1c). Another source of uncertainty is the error in the differential DEM. It is

TCD
7, 841–871, 2013

estimated using the standard deviation of the elevation differences against ICESat data (1.6 m for Spot5, 11.7 m for ASTER). The error on the elevation change over the lake area is obtained by dividing 11.8 m (the square root of the sum of the squares of 1.6 m and 11.7 m) by the square root of the number of independent pixels in the Lake $Cook_{E2}$ area (Bretherton et al., 1999) using an auto-correlation length of 1 km (Berthier et al., 2012; Nuth and Kääb, 2011). The correlation length cannot be estimated specifically for this study because of the lack of stable terrain but our value is conservative because shorter lengths have previously been used with similar dataset (500 m in Berthier et al., 2010; 200 m in Howat et al., 2008). This elevation change error is ±0.22 m and, multiplied by the area of the lake, leads to a total DEM error of $\pm 0.05\,km^3$ of water. These "lake area" and DEM errors cannot be considered independent and hence, the total uncertainty is the arithmetic sum of the two, leading to a total uncertainty of $0.15\,km^3$. $4.52 \pm 0.15\,km^3$ represents the net loss between early 2006 and early 2012 and thus, underestimates the total volume of water discharged during the event itself given that the ice sheet surface rose between October 2008 and February 2012 (Fig. 2). Using the elevation differences between ICESat 2E and the SPOT5 DEM (Fig. 1c), we estimate that the volume change was $+0.64\,km^3$ between October 2009 and February 2012. The error on the latter value is difficult to estimate formally, so a conservative 50% error is assumed. Thus, in total, the discharge is estimated to be: $4.52 \pm 0.15 + 0.64 \pm 0.32 = 5.16 \pm 0.47\,km^3$.

4 Subsequent cascade of lakes

Smith et al. (2009) pointed out a possible connection between $Cook_{E2}$ and $Cook_{E1}$, located a hundred kilometers downstream. To further investigate the effect of the $5.2\,km^3$ of water that drained out of $Cook_{E2}$, we analyzed a map of elevation changes for the Wilkes Land derived from Envisat (Flament and Rémy, 2012). This map features an intriguing pattern downstream of Lake $Cook_{E2}$, with spots of very local uplift in a region of overall negative elevation trend (Fig. 3).

TCD
7, 841–871, 2013

Most active lakes can be identified on this map of elevation trends due to their positive elevation trend because the surrounding area is either stable or of slightly declining elevation. The positive elevation trend does not necessarily mean that the lakes permanently stored water from Lake $Cook_{E2}$, as can be seen on the series of Lake $Cook_{E1}$ (Fig. 3a). Lake $Cook_{E2}$ drainage and the subsequent passage of water through downstream lakes happened during the second half of the Envisat observation period; consequently a trend fitted through the full time series is positive, even though the surface elevation returned to the pre-drainage level after the passage of water. Starting from Lake $Cook_{E2}$, active lakes are aligned along a curved line first oriented northward before bending to the northwest approximately at the middle of the path. In order to confirm this apparent flowpath, we used the BEDMAP2 dataset (Fretwell et al., 2013) to compute the most likely routes for water draining from Lake $Cook_{E2}$.

Our goal in the following was to perform a water budget and verify that the volume of water that was stored transitorily or permanently in the downstream region of Lake $Cook_{E2}$ is similar in magnitude to the amount of water that drained from Lake $Cook_{E2}$. To do so we needed, first, to restrict our analysis to the area hydrologically-connected to Lake $Cook_{E2}$ (see Sect. 4.1) and, second, to find an algorithm to automatically detect active lakes in the map of elevation trends (Sect. 4.2).

4.1 Subglacial water flowpath inferred from BEDMAP2

Following Carter et al. (2011), we assumed that the hydropotential at the ice sheet base is a function of the bedrock elevation and the thickness of the overlying ice column. With the assumption that water will flow following the steepest gradient of the hydropotential, we can compute possible flowpaths for the water draining from Lake $Cook_{E2}$. From the BEDMAP2 bedrock elevation map and ice thickness, we compute the hydropotential (H_p) as:

$$H_p = g\rho_w h_b + g\rho_i (h_s - h_b)$$

TCD
7, 841–871, 2013

where ρ_w and ρ_i are, respectively the densities of water and ice, and h_b and h_s the elevations of the bed and the ice-sheet surface. We thus obtain a map of hydropotential with a 1 km grid spacing from which we can derive flowpaths. We choose to use a gradient descent algorithm, starting from Lake Cook_{E2}. The slope of the hydropotential is computed by fitting a plane on a disc of 10 km-radius and taking steps of 7 km in the direction of steepest descent. In order to account for the errors in the BEDMAP2 dataset, we use a Metropolis-Hastings algorithm (Hastings, 1970): we allow the step direction to vary around the direction of steepest descent, proportionally to the accuracy provided with the map of the bedrock, i.e. the greater the uncertainty in the bedrock elevation, the greater the angle by which the descent direction is allowed to vary. We then draw 10 000 flowpaths to obtain a large set of lines. The result is aggregated in Fig. 4.

4.2 Automatic identification of active lakes

We propose to fit the elevation time series with Gaussian curves with varying start dates, widths and amplitudes to automatically detect and determine the characteristics of these lakes. The algorithm is applied to a zone covering all flowpaths derived from BEDMAP2 plus a 20 km buffer zone on each side. The buffer zone is needed here to analyze an area larger than the one strictly covered by the computed flowpaths to take into account the uncertainty in the methodology and in the subglacial topography. It prevents rejecting some lakes, such as Lake Cook_{E1} which lies in a trough out of reach of our water routing algorithm. The lake-detection algorithm assigns a start date, an amplitude and a flood duration to each time-series along with the correlation to the fitted Gaussian curve. If this correlation is higher than a given correlation threshold (ranging between 0.6 and 0.9), the algorithm detected a potential lake. The screening of the lake candidates is then refined using the following criteria:

- The start date of the event, defined as the peak date of the Gaussian curve minus one standard deviation, must not be too early. The earliest allowed start date is 2006.85 (see Sect. 5.2).

TCD
7, 841–871, 2013

– The series must not be too noisy. Noise is computed as the standard deviation of the raw series minus the 11-point moving average smoothed series. The noise level must be below 1 m.

– The series must have enough samples (a minimum of 70 out of 85).

The result of this selection is shown in Fig. 5. The start dates in this figure increase as altitude decreases, in good agreement with the natural flow direction of sub-glacial water. After performing this fit, all computations (e.g. cumulative volume of water) are performed using the full time series. The fitted Gaussian curve was only used for the automatic detection.

Elevation time series of all detected lakes downstream of Lake $Cook_{E2}$ are converted to volume and summed. The result is plotted in Fig. 6. The elevation series are smoothed with an 11-point moving average and set to 0 on 2006.85 to provide a common reference date. To convert elevation time series to volume, we approximate the area covered by each time series at 12 km^2 because the area of interest covers 50 000 km^2 and is sampled by 4220 time series.

We consider the post-drainage volume at "lake points" as the water volume, neglecting other influences on the surface elevation. Thus, this volume also includes all surface elevation changes, mostly due to changes in surface mass balance that cannot be separated from the elevation changes driven by the subglacial lake filling/drainage. The variation in volume prior to the start of the drainage shows that they can account for a significant part of the changes, attributed to the drainage of subglacial water.

The "volume stored in lakes" (curve "0.6" on Fig. 6) is slightly negative before the drainage with a small annual cycle, some inter-annual variations and a minimum volume during 2004. The flood event is clearly seen between early-2007 and mid-2008. The peak volume, up to 4.47 km^3 if the correlation threshold is set to 0.6, is reached during the austral winter of 2008. After the peak, water continues to drain from the lakes and the volume stored at the beginning of 2010 is only slightly greater than 2 km^3. Table 1 highlights the strong sensitivity of our volume estimate to the correlation threshold.

TCD
7, 841–871, 2013

5 Discussion

5.1 Usefulness of DEM derived from stereo-imagery in central Antarctica

A nearly complete surface topography of the Lake $Cook_{E2}$ area was derived from a SPOT5 stereo pair with a precision greater than ±2 m at the 1-sigma level after adjustment against ICESat data. This is a promising result for the central plateau of the East Antarctic Ice Sheet where DEMs derived from stereo-imagery have been of little use up to now and thus have often been replaced by photoclinometry (e.g. Bindschadler et al., 2011). Because of their limited coverage and the associated cost, DEMs from SPOT5 (or other sensors with similar stereo capabilities) cannot currently replace frequent passages of the laser and radar altimeters to continuously monitor elevation changes of the whole ice sheet but can be helpful to better describe some discrete events, such as subglacial lake drainages. In the case of Lake $Cook_{E2}$, our sequential DEM analysis provided a more reliable estimate of the amount of water that drained from the lake than a previous one purely based on ICESat data. The DEM and the associated imagery also revealed that the lake shape is not elliptical, which was a natural assumption based on ICESat measurements alone. In total, over 5 km^3 of water drained in about 2 yr, the largest event reported so far under the Antarctic ice sheet.

5.2 Ability of classic radar altimetry to capture the drainage of Lake $Cook_{E2}$

The high spatial resolution provided by DEMs is complemented by the temporal resolution of nadir pointing altimetry. The small footprint of ICESat laser altimeter (around 70 m) is better suited than the approximately 10 km footprint of Envisat radar altimeter for observing the drainage of Lake $Cook_{E2}$. The lake size being commensurable with the diameter of the Envisat altimeter footprint, the altimeter is not able to retrieve any echo from the bottom of the trough left by the lake drainage (see Fig. 7a). The tracking system would probably not be able to follow such an abrupt change in slope either. The difference in elevation shown in the figure is in fact a misinterpreted difference in

TCD
7, 841–871, 2013

radar range: as the lake trough deepens, the point sending back the first echo is not at nadir any more but has shifted towards the rim of the depression, which yields a longer range. The minimum distance from a nadir point at the center of the depression to the lake margin is about 5 km (e.g. for the time series in Fig. 7). For a 5 km shift and a satellite altitude of 800 km, the range difference is 15.6 m. This is in remarkable agreement with Fig. 7a if we take into account that the echo is expected to be strongly distorted in such a situation. Because of this limitation, inherent to classic radar altimetry, no accurate estimate of the lake drainage can be done from Envisat measurements. The along-track processing we described earlier is only the fit of a simple model and cannot correct the large topographic modifications due to the lake drainage. It explains the large noise level (1.4 m) in the time series shown in Fig. 7a. However, if we use only measurements from the pre-drainage period, the simple quadratic model for the surface topography performs much better (Fig. 7b). From this shortened time series with a noise level of 0.1 m, it is possible to detect accurately the first large perturbation of surface elevation, around 2006.85, our best estimate for the start of the drainage.

Downstream of Lake Cook_{E2}, elevation changes are less abrupt and can be monitored using Envisat. Envisat coverage is temporally denser than ICESat (regular 35-day cycle for Envisat versus 2–3 measurements a year with ICESat). This compensates for the slightly higher noise in the time series of the radar altimeter. ICESat has a single point accuracy of 10–15 cm (Shuman et al., 2006; Brenner et al., 2007) whereas noise in the Envisat series after along-track processing and in the area of interest here is about 20 cm. Large events, clearly standing out of the noise, can also be more precisely dated due to the high repetition rate of Envisat measurements.

5.3 Ability to close the subglacial water budget

Frequently repeated altimetry measurements combined with DEM differencing provided a detailed view on the drainage of Lake Cook_{E2} and an improved estimate of the water discharge. Before water reaches the coast, we expect to find nearly all of the drained volume temporarily stored in the downstream lakes. The water budget is

TCD
7, 841–871, 2013

approximately closed, yet the error on the volume stored downstream is high and there is a high sensitivity of our estimate to the correlation threshold. Several sources contribute to the error:

(i) The "lake signal" is mixed up with elevation changes from other phenomena acting on the ice sheet surface. In particular, it is a difficult problem to compensate for the natural variability in snowfalls. Snowfall variability produces elevation change signals on interannual time scales (Lenaerts et al., 2012; Magand et al., 2007), comparable to the lake drainage time scales. Most time series that were rejected because of a too early "start date" (Fig. 5) had a good correlation to a Gaussian curve that was due to decimeter-scale elevation variations on interannual timescales. We expect this type of time series to reflect accumulation variation. Faint displacements due to lakes are mixed up with this signal and both cannot be accurately separated. It could be a large contribution to the difference between the volume that drained from Lake Cook_{E2} and the estimate of the volume stored in downstream lakes.

(ii) It is possible that part of the water flowed rapidly through well-carved channels and did not leave a persistent imprint on the surface.

(iii) Faint signals could go undetected. This could be a large contribution if water was stored as a thin layer over a large area.

(iv) Finally, some water probably reached the coast towards mid-2008 and exited our investigation area before Lake Cook_{E2} completely drained.

However, at the peak date more than 88 % of the volume drained from Lake Cook_{E2} is found downstream. It implies that most of the water flowing underneath the ice sheet had a direct impact on the surface elevation, and that this impact was large enough to be detected by Envisat radar altimetry.

The observation period is too short to infer anything about a cyclic behavior of Lake Cook_{E2}. However, the MODIS Mosaic Of Antarctica, acquired over winter 2003–2004,

TCD
7, 841–871, 2013

i.e. before the start of the drainage, reveals a faint feature on the ice sheet surface, similar to the lake contours (Fig. 8). This surface feature could have been created by the accumulation of water preceding the drainage, or by a previous drainage.

5.4 Uplift of the glacier surface since 2009

The comparison between the February 2012 SPOT 5 DEM and the last ICESat measurement in late 2009 reveals that the center depression has risen by about 13 ± 1.6 m in two and a half years. Several processes can potentially have contributed to the surface rising: water refilling the subglacial cavity, accumulation of windblown snow or local ice flow convergence.

By the same method used to estimate the downstream flowpaths from Lake Cook_{E2}, we can determine the flowpaths converging toward Lake Cook_{E2}. Starting from a pixel at the rim of the lake depression, we systematically explore the lake surroundings: from a given pixel, we draw a 100 flow paths going down the hydropotential. If more than a given percent of these flow paths reach the lake, the pixel is considered part of the drainage basin of Lake Cook_{E2} and all of its 8 neighbors are added to the list of pixels to be tested. The exploration stops when no pixel is left in the list. We consider the most likely drainage basin is the zone with more than 50 % chance to reach the lake ($530\,\text{km}^2$) plus the lake area ($220\,\text{km}^2$). The areas with 95 % and 5 % chance to reach the lake give our uncertainty margin, respectivelly $230\,\text{km}^2$ and $1030\,\text{km}^2$.

The resulting water collection area is about $750 \pm 300\,\text{km}^2$. The small size of this collecting basin can be explained by the proximity of the ridge leading to Talos Dome. The observed refilling of $0.64 \pm 0.32\,\text{km}^3$ in 3 yr would imply a basal melt rate between $0.3\,\text{m yr}^{-1}$ (refilling of $0.32\,\text{km}^3$ and a basin of $1050\,\text{km}^2$) and $2\,\text{m yr}^{-1}$ (refilling of $0.96\,\text{km}^3$ and a basin of $450\,\text{km}^2$). These values are at least two orders of magnitude higher than expected values in this region (Pattyn, 2010).

The hypothesis of the depression filling by windblown snow is difficult to test. One could expect that snow transport close to a ridge is small because the katabatic winds are unlikely to be strong there. However, the large topographic anomaly left by the

TCD
7, 841–871, 2013

drainage could still perturb near-surface winds and contribute to the accumulation of snow. We cannot formally exclude this hypothesis.

The last possibility, filling of the trough by local ice flow convergence (e.g. Adalgeirsdottir et al., 2000), could be the dominant phenomenon. The depression "refills" at a rate of 0.2 $km^3 yr^{-1}$. Given its 70 km long rim and a 2700 m thick ice column, this ice flux corresponds to a 1 $m yr^{-1}$ change in average ice flow velocity. At this location, the annual velocity is about 5 ± 5 $m yr^{-1}$ (Rignot et al., 2011).

5.5 Bias on the regional trend in surface elevation

Finally, on many lakes downstream of Lake $Cook_{E2}$, the flood event produced a temporary rise of the surface. As these events happened during the second half of the Envisat observation period, they produced an artificial positive elevation change signal when a linear trend is fitted to the time series. This is a good example showing that long and continuous observations are needed to better understand long-term trends and that care must be taken if the time series are not analyzed in more detail.

6 Conclusions

A major drainage event was detected by radar and laser altimetry and analyzed in detail with DEMs derived from stereo-imagery in the Wilkes Land, East Antarctica. This dramatic drainage lasted 2 yr, occurred under 2700 m of ice, led to a surface lowering of up to 70 m, affected a total area of about 220 km^2 and released over 5 km^3 of water. The peak discharge rate, at 80 $m^3 s^{-1}$ is larger than reported in earlier similar events underneath the Antarctic Ice sheet and was sustained during more than 1 yr. However, this discharge rate remained 1–2 order of magnitude smaller than peak discharge rate of outburst flood in Iceland (Björnsson, 2003). Surface features were present on optical imagery prior to this event, suggesting that this region is hydrologically active and could be subject to recurring drainage. It will be of great interest to monitor the evolution of this

TCD
7, 841–871, 2013

deep depression in the future using ongoing (Cryosat-2) or future altimetry missions (SARAL/AltiKa on the same orbit as Envisat or ICESat-2, Sentinel-3 on different orbits). The study of such local and rapid events is only possible with both sufficient temporal and spatial resolution and continuous coverage.

ICESat laser altimetry yields better observations of the drainage at Lake $Cook_{E2}$ as Envisat radar altimetry is not able to observe the bottom of the trough left after the water has flowed away. Still, the absence of cross-track coverage from ICESat precludes an accurate computation of the volume drained from the lake. The dense temporal sampling of Envisat permits to constrain the date of the start of the drainage. Envisat radar altimetry also revealed a complex pattern of elevation changes downstream of Lake $Cook_{E2}$ and we interpret them as the surface expression of transient storage of water in a succession of subglacial lakes. In particular, observations of transient storage/release of water in lakes located relatively close to the coast suggest that part of the water released by Lake $Cook_{E2}$ reached the southern ocean after travelling over 500 km underneath the ice sheet.

Outlet glaciers flowing in the Cook Ice Shelf are flowing over the deep Wilkes subglacial basin, where bedrock depth is far below sea level (Fretwell et al., 2013). Marine ice-sheet are suspected to be the most prone to collapse in a warming climate (e.g. Durand et al., 2009). Future studies should aim to determine whether this large amount of water influenced the flow of ice, in particular for the eastern tributary of Cook Ice Shelf.

Acknowledgements. T.F's Ph.D. grant is funded by the French Space Agency (CNES) and the Centre National de la Recherche Scientifique (CNRS). E.B. acknowledges support from the CNES through the TOSCA and from the Programme National de Télédétection Spatiale. SPOT 5 images and DEMs were available at reduced cost thanks to support from CNES through ISIS project 639.

TCD
7, 841–871, 2013

The publication of this article is financed by CNRS-INSU.

References

Aðalgeirsdóttir, G., Gudmundsson, G. H., and Björnsson, H.: The response of a glacier to a surface disturbance: a case study on Vatnajökull ice cap, Iceland, Ann. Glaciol., 31, 104–110, doi:10.3189/172756400781819914, 2000.

Bamber, J. L., Gomez-Dans, J. L., and Griggs, J. A.: A new 1 km digital elevation model of the Antarctic derived from combined satellite radar and laser data – Part 1: Data and methods, The Cryosphere, 3, 101–111, doi:10.5194/tc-3-101-2009, 2009.

Bell, R. E., Studinger, M., Shuman, C. A., Fahnestock, M. A., and Joughin, I.: Large subglacial lakes in East Antarctica at the onset of fast-flowing ice streams, Nature, 445, 904–907, doi:10.1038/nature05554, 2007.

Berthier, E., Schiefer, E., Clarke, G. K. C., Menounos, B., and Rémy, F.: Contribution of Alaskan glaciers to sea-level rise derived from satellite imagery, Nature Geosci., 3, 92–95, doi:10.1038/ngeo737, 2010.

Berthier, E., Scambos, T. A., and Shuman, C. A.: Mass loss of Larsen B tributary glaciers (Antarctic Peninsula) unabated since 2002, Geophys. Res. Lett., 39, L13501, doi:10.1029/2012GL051755, 2012.

Bindschadler, R., Choi, H., Wichlacz, A., Bingham, R., Bohlander, J., Brunt, K., Corr, H., Drews, R., Fricker, H., Hall, M., Hindmarsh, R., Kohler, J., Padman, L., Rack, W., Rotschky, G., Urbini, S., Vornberger, P., and Young, N.: Getting around Antarctica: new high-resolution mappings of the grounded and freely-floating boundaries of the Antarctic ice sheet created for the International Polar Year, The Cryosphere, 5, 569–588, doi:10.5194/tc-5-569-2011, 2011.

TCD
7, 841–871, 2013

Björnsson, H.: Subglacial lakes and jökulhlaups in Iceland, Global Planet. Change, 35, 255–271, doi:10.1016/S0921-8181(02)00130-3, 2003.
Brenner, A. C., DiMarzio, J. P., and Zwally, H. J.: Precision and accuracy of satellite radar and laser altimeter data over the continental ice sheets, IEEE T. Geosci. Remote, 45, 321–331, doi:10.1109/TGRS.2006.887172, 2007.
Bretherton, C. S., Widmann, M., Dymnikov, V. P., Wallace, J. M., and Bladé, I.: The effective number of spatial degrees of freedom of a time-varying field, J. Climate, 12, 1990–2009, doi:10.1175/1520-0442(1999)012<1990:TENOSD>2.0.CO;2, 1999.
Carter, S. P., Fricker, H. A., Blankenship, D. D., Johnson, J. V., Lipscomb, W. H., Price, S. F., and Young, D. A.: Modeling 5 years of subglacial lake activity in the MacAyeal Ice Stream (Antarctica) catchment through assimilation of ICESat laser altimetry, J. Glaciol., 57, 1098–1112, doi:10.3189/002214311798843421, 2011.
Clarke, G. K. C.: Glaciology: ice-sheet plumbing in Antarctica, Nature, 440, 1000–1001, doi:10.1038/4401000a, 2006.
Durand, G., Gagliardini, O., De Fleurian, B., Zwinger, T., and Le Meur, E.: Marine ice sheet dynamics: hysteresis and neutral equilibrium, J. Geophys. Res., 114, F03009, doi:10.1029/2008JF001170, 2009.
Flament, T. and Rémy, F.: Dynamic thinning of Antarctic glaciers from along-track repeat radar altimetry, J. Glaciol., 58, 830–840, 2012.
Fretwell, P., Pritchard, H. D., Vaughan, D. G., Bamber, J. L., Barrand, N. E., Bell, R., Bianchi, C., Bingham, R. G., Blankenship, D. D., Casassa, G., Catania, G., Callens, D., Conway, H., Cook, A. J., Corr, H. F. J., Damaske, D., Damm, V., Ferraccioli, F., Forsberg, R., Fujita, S., Gim, Y., Gogineni, P., Griggs, J. A., Hindmarsh, R. C. A., Holmlund, P., Holt, J. W., Jacobel, R. W., Jenkins, A., Jokat, W., Jordan, T., King, E. C., Kohler, J., Krabill, W., Riger-Kusk, M., Langley, K. A., Leitchenkov, G., Leuschen, C., Luyendyk, B. P., Matsuoka, K., Mouginot, J., Nitsche, F. O., Nogi, Y., Nost, O. A., Popov, S. V., Rignot, E., Rippin, D. M., Rivera, A., Roberts, J., Ross, N., Siegert, M. J., Smith, A. M., Steinhage, D., Studinger, M., Sun, B., Tinto, B. K., Welch, B. C., Wilson, D., Young, D. A., Xiangbin, C., and Zirizzotti, A.: Bedmap2: improved ice bed, surface and thickness datasets for Antarctica, The Cryosphere, 7, 375–393, doi:10.5194/tc-7-375-2013, 2013.
Fricker, H. A. and Scambos, T.: Connected subglacial lake activity on lower Mercer and Whillans Ice Streams, West Antarctica, 2003–2008, J. Glaciol., 55, 303–315, doi:10.3189/002214309788608813, 2009.

TCD
7, 841–871, 2013

Fricker, H. A., Scambos, T. A., Bindschadler, R., and Padman, L.: An active subglacial water system in West Antarctica mapped from space, Science, 315, 1544–1548, doi:10.1126/science.1136897, 2007.
Gardelle, J., Berthier, E., and Arnaud, Y.: Slight mass gain of Karakoram glaciers in the early twenty-first century, Nature Geosci., 5, 322–325, doi:10.1038/ngeo1450, 2012.
Gray, L., Joughin, I., Tulaczyk, S., Spikes, V. B., Bindschadler, R., and Jezek, K.: Evidence for subglacial water transport in the West Antarctic Ice Sheet through three-dimensional satellite radar interferometry, Geophys. Res. Lett., 32, L03501, doi:10.1029/2004GL021387, 2005.
Hastings, W. K.: Monte Carlo sampling methods using Markov chains and their applications, Biometrika, 57, 97–109, doi:10.1093/biomet/57.1.97, 1970.
Howat, I. M., Joughin, I., and Scambos, T. A.: Rapid changes in ice discharge from Greenland outlet glaciers, Science, 315, 1559–1561, doi:10.1126/science.1138478, 2007.
Howat, I. M., Smith, B. E., Joughin, I., and Scambos, T. A.: Rates of southeast Greenland ice volume loss from combined ICESat and ASTER observations, Geophys. Res. Lett., 35, L17505, doi:10.1029/2008GL034496, 2008.
Joughin, I., Tulaczyk, S., MacAyeal, D. R., and Engelhardt, H.: Melting and freezing beneath the Ross ice streams, Antarctica, J. Glaciol., 50, 96–108, doi:10.3189/172756504781830295, 2004.
Korona, J., Berthier, E., Bernard, M., Rémy, F., and Thouvenot, E.: SPIRIT. SPOT 5 stereoscopic survey of Polar Ice: reference images and topographies during the fourth International Polar Year (2007–2009), ISPRS J. Photogramm., 64, 204–212, doi:10.1016/j.isprsjprs.2008.10.005, 2009.
Lenaerts, J. T. M., Van den Broeke, M. R., Van de Berg, W. J., Van Meijgaard, E., and Kuipers Munneke, P.: A new, high-resolution surface mass balance map of Antarctica (1979–2010) based on regional atmospheric climate modeling, Geophys. Res. Lett., 39, L04501, doi:10.1029/2011GL050713, 2012.
Magand, O., Genthon, C., Fily, M., Krinner, G., Picard, G., Frezzotti, M., and Ekaykin, A. A.: An up-to-date quality-controlled surface mass balance data set for the 90°–180° E Antarctica sector and 1950–2005 period, J. Geophys. Res., 112, D12106, doi:10.1029/2006JD007691, 2007.
Moholdt, G., Nuth, C., Hagen, J. O., and Kohler, J.: Recent elevation changes of Svalbard glaciers derived from ICESat laser altimetry, Remote Sens. Environ., 114, 2756–2767, doi:10.1016/j.rse.2010.06.008, 2010.

TCD
7, 841–871, 2013

Nuth, C. and Kääb, A.: Co-registration and bias corrections of satellite elevation data sets for quantifying glacier thickness change, The Cryosphere, 5, 271–290, doi:10.5194/tc-5-271-2011, 2011.
Pattyn, F.: Antarctic subglacial conditions inferred from a hybrid ice sheet/ice stream model, Earth Planet. Sc. Lett., 295, 451–461, doi:10.1016/j.epsl.2010.04.025, 2010.
Rignot, E., Mouginot, J., and Scheuchl, B.: Ice flow of the Antarctic ice sheet, Science, 333, 1427–1430, doi:10.1126/science.1208336, 2011.
Scambos, T. A., Haran, T. M., Fahnestock, M. A., Painter, T. H., and Bohlander, J.: MODIS-based Mosaic of Antarctica (MOA) data sets: continent-wide surface morphology and snow grain size, Remote Sens. Environ., 111, 242–257, doi:10.1016/j.rse.2006.12.020, 2007.
Scambos, T. A., Berthier, E., and Shuman, C. A.: The triggering of subglacial lake drainage during rapid glacier drawdown: Crane Glacier, Antarctic Peninsula, Ann. Glaciol., 52, 74–82, doi:10.3189/172756411799096204, 2011.
Schoof, C.: Ice-sheet acceleration driven by melt supply variability, Nature, 468, 803–806, doi:10.1038/nature09618, 2010.
Shuman, C. A., Zwally, H. J., Schutz, B. E., Brenner, A. C., DiMarzio, J. P., Suchdeo, V. P., and Fricker, H. A.: ICESat Antarctic elevation data: Preliminary precision and accuracy assessment, Geophys. Res. Lett., 33, L07501, doi:10.1029/2005GL025227, 2006.
Siegert, M. J.: Lakes beneath the ice sheet: the occurrence, analysis, and future exploration of Lake Vostok and other antarctic subglacial lakes, Ann. Rev. Earth. Planet. Sci., 33, 215–245, doi:10.1146/annurev.earth.33.092203.122725, 2005.
Siegert, M. J. and Dowdeswell, J. A.: Spatial variations in heat at the base of the Antarctic ice sheet from analysis of the thermal regime above subglacial lakes, J. Glaciol., 42, 501–509, 1996.
Smith, B. E., Fricker, H. A., Joughin, I. R., and Tulaczyk, S.: An inventory of active subglacial lakes in Antarctica detected by ICESat (2003–2008), J. Glaciol., 55, 573–595, doi:10.3189/002214309789470879, 2009.
Sørensen, L. S., Simonsen, S. B., Nielsen, K., Lucas-Picher, P., Spada, G., Adalgeirsdottir, G., Forsberg, R., and Hvidberg, C. S.: Mass balance of the Greenland ice sheet (2003–2008) from ICESat data – the impact of interpolation, sampling and firn density, The Cryosphere, 5, 173–186, doi:10.5194/tc-5-173-2011, 2011.

TCD
7, 841–871, 2013

Stearns, L. A., Smith, B. E., and Hamilton, G. S.: Increased flow speed on a large East Antarctic outlet glacier caused by subglacial floods, Nature Geosci., 1, 827–831, doi:10.1038/ngeo356, 2008.

Toutin, T.: ASTER DEMs for geomatic and geoscientific applications: a review, Int. J. Remote Sens., 29, 1855–1875, doi:10.1080/01431160701408477, 2008.

Wingham, D. J., Siegert, M. J., Shepherd, A., and Muir, A. S.: Rapid discharge connects Antarctic subglacial lakes, Nature, 440, 1033–1036, doi:10.1038/nature04660, 2006.

TCD
7, 841–871, 2013

Table 1. Properties of the estimated volume of water downstream of Lake $Cook_{E2}$ for different values of "correlation threshold" (see text).

Correlation threshold	Peak volume, km^3	Peak date	Minimum before the flood, km^3	RMS before the flood, km^3	Number of "lake points"
0.6	4.47	Jun 2008	−1.51	0.85	760
0.7	4.13	Jun 2008	−1.31	0.79	638
0.8	3.16	Jun 2008	−1.09	0.69	505
0.9	2.97	Jul 2008	−0.73	0.47	331

TCD
7, 841–871, 2013

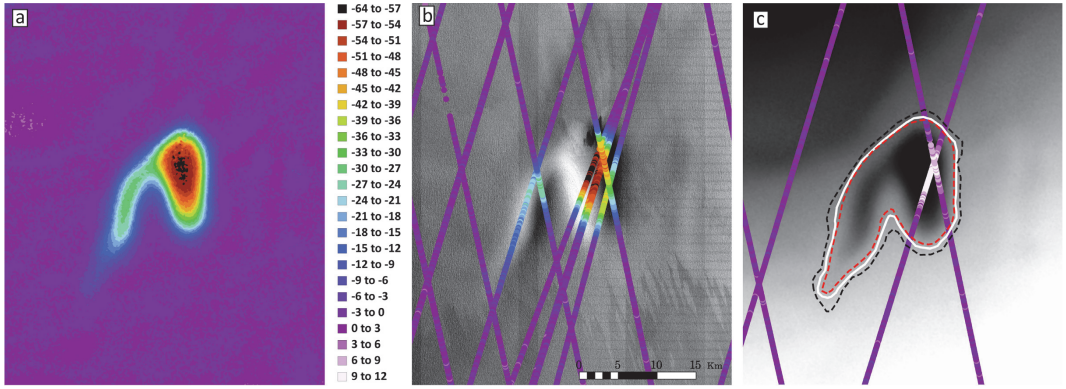

Fig. 1. Elevation difference (m) for Lake $Cook_{E2}$ from ICESat, SPOT5 and ASTER DEMs. Negative values correspond to surface lowering. Elevation changes on all panels share the same color scale. **(a)** Map of elevation differences between the post- and pre-drainage DEMs. **(b)** Elevation difference between the 9 February 2012 SPOT5 DEM and ICESat laser periods 2A, 3B and 3C, all acquired prior to the lake drainage. These laser periods were selected to illustrate the evolving spatial sampling of the surface lowering that can be obtained from different laser periods. Note that only laser period 2A crosses the secondary lake. Background; the SPOT5 image from 9 February 2012 (copyright: CNES 2012, distribution Spot Image). **(c)** Elevation difference between the 9 February 2012 SPOT5 DEM and ICESat laser periods 2E, acquired in March 2009, after the lake drainage. The black, white, and red lines that materialize the rim around the depression represent elevation difference thresholds of −1.5 m, −3 m, and −5.5 m, respectively. The corresponding "lake area" is, respectively, 267 km^2, 219 km^2 and 192 km^2. This panel shows the approximately 10–15 m rise of the surface above Lake $Cook_{E2}$ during the 4 yr following the drainage. Background: the 9 February 2012 SPOT5 DEM.

TCD
7, 841–871, 2013

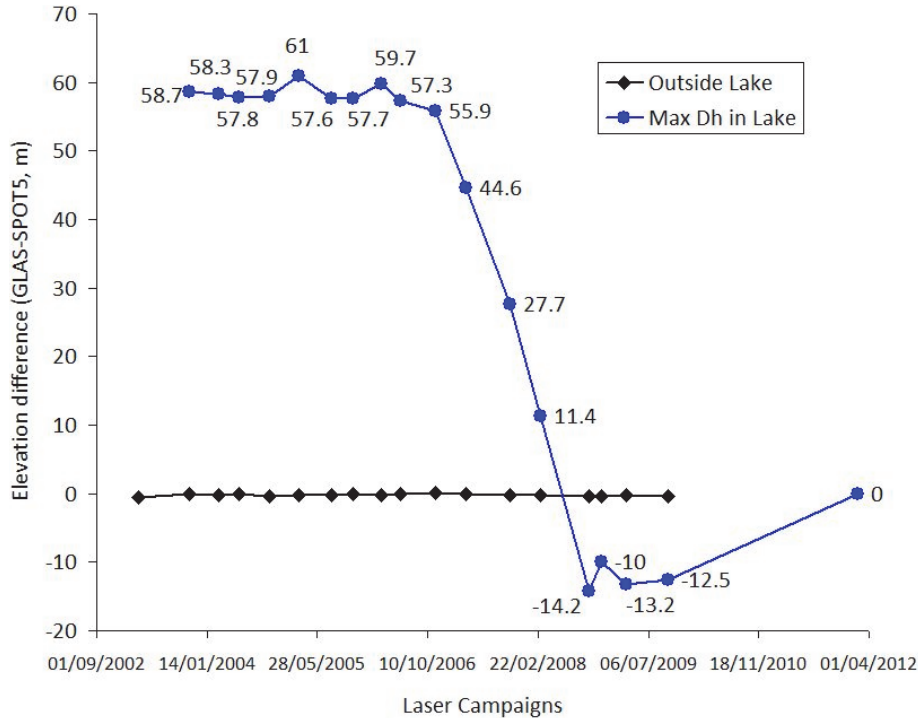

Fig. 2. Time series of elevation difference between the various ICESat laser periods and the 9 February 2012 SPOT5 DEM. In black, the mean elevation difference outside of Lake $Cook_{E2}$. In blue, the maximum elevation difference between ICESat and the DEM. Note that due to non-perfect repetitiveness of ICESat tracks, the blue dots do not correspond to the same location for each laser campaign (Fig. 1b) which explains why the noise seems larger within the Lake $Cook_{E2}$ area than outside.

TCD
7, 841–871, 2013

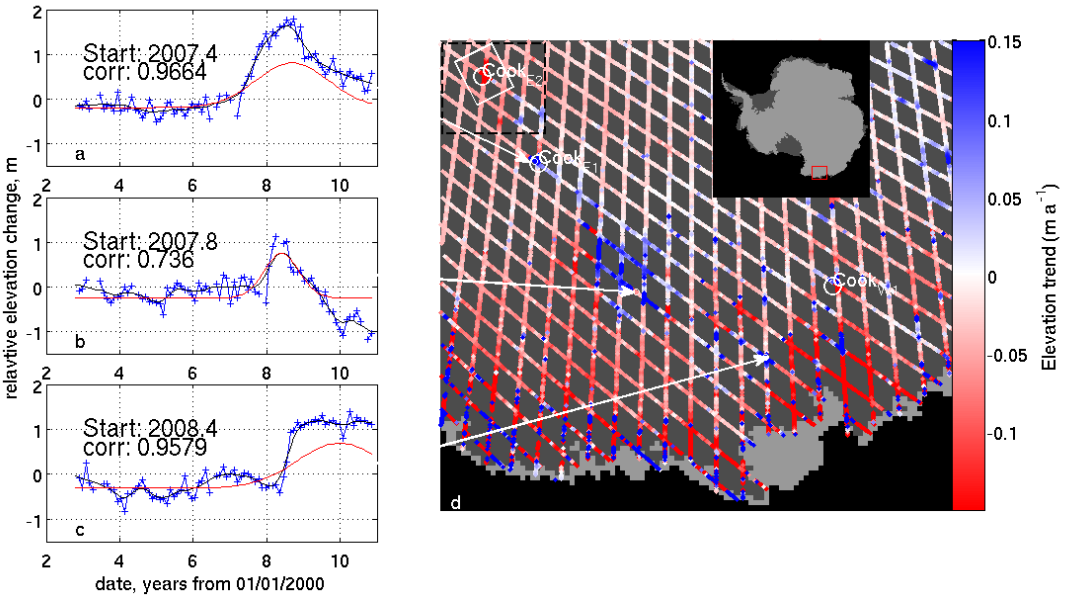

Fig. 3. (a–c) Time-series of relative elevation difference for 3 different locations along the flow path. **(a)** shows the time series for Lake $Cook_{E1}$. **(d)** Elevation trend along Envisat tracks overlaid on a MODIS Mosaic of Antarctica (Scambos et al., 2007). The black dashed line box delineates Fig. 8 and the white box delineates Fig. 1. X- and y-axes are given in m in the south polar stereographic projection (EPSG:3031). Four lakes reported by Smith et al. (2009) in the area are indicated with a white circle. The Cook Ice Shelf, after which the lakes were named, is in the lower right corner.

TCD
7, 841–871, 2013

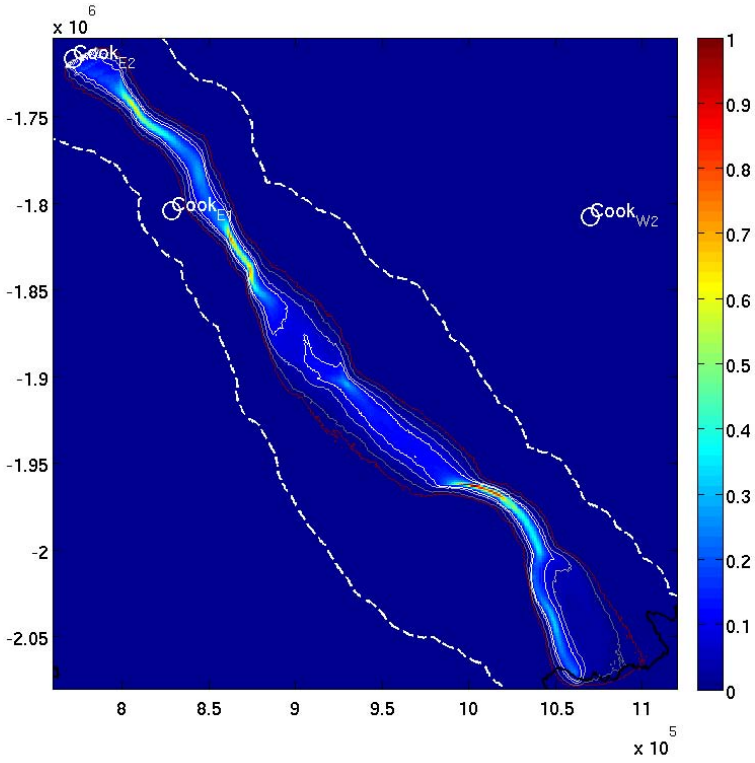

Fig. 4. Relative probability for water to flow through one pixel. The pixel with highest probability is set to 1. The contours encompass the 0.1 (white), 0.05 (light grey), 0.01 (darker grey) and 0.001 (dark red) probability. Lakes reported by Smith et al. (2009) are plotted as white circles. Note that Lake Cook_{E1} is outside of the most likely flowpaths because it stands in a small and deep trough not resolved by our routing algorithm. The white dashed line is the search area (defined in Sect. 4.2).

TCD
7, 841–871, 2013

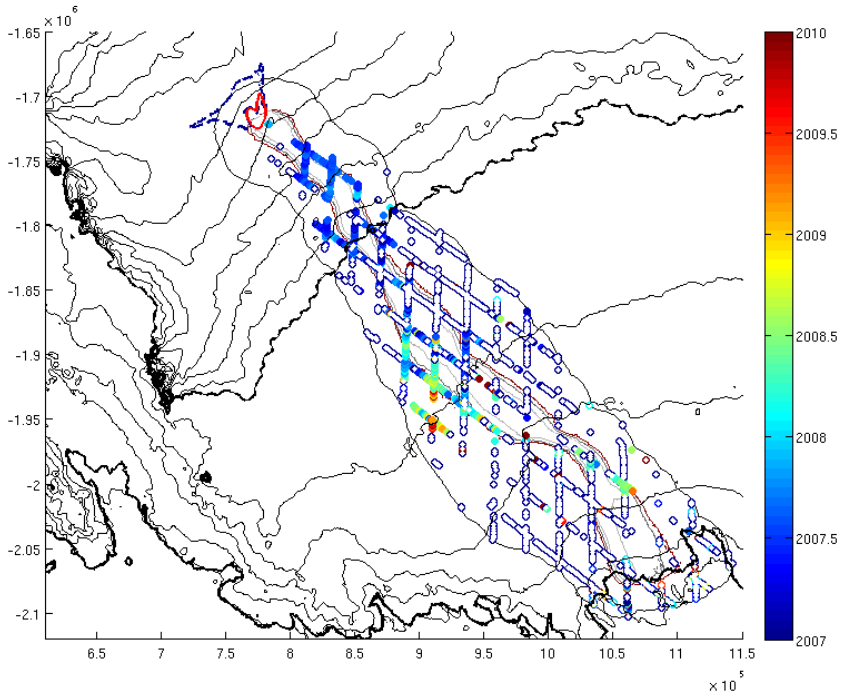

Fig. 5. Start date of the filling for sub-glacial lakes in the hydrologically-connected area downstream of the Lake Cook_{E2}. The edges of the probable flowpath are reproduced from Fig. 4 and the black line encompassing all lakes shows the limits of our search area (defined in Sect. 4.2). Elevation contour from the Bamber et al. (2009) DEM are superimposed every 400 m up to 2000 m elevation (dashed bold line) and every 50 m above this line. The drainage basin of Lake Cook_{E2} (5 % probability to reach the lake, see Sect. 5.4) is plotted in dashed blue line and the lake contour (−3 m) is in red. The start date of the flood is indicated for all active lakes. Points marked with a white dot were initially flagged as lakes but then rejected during the second round of selection, see text.

TCD
7, 841–871, 2013

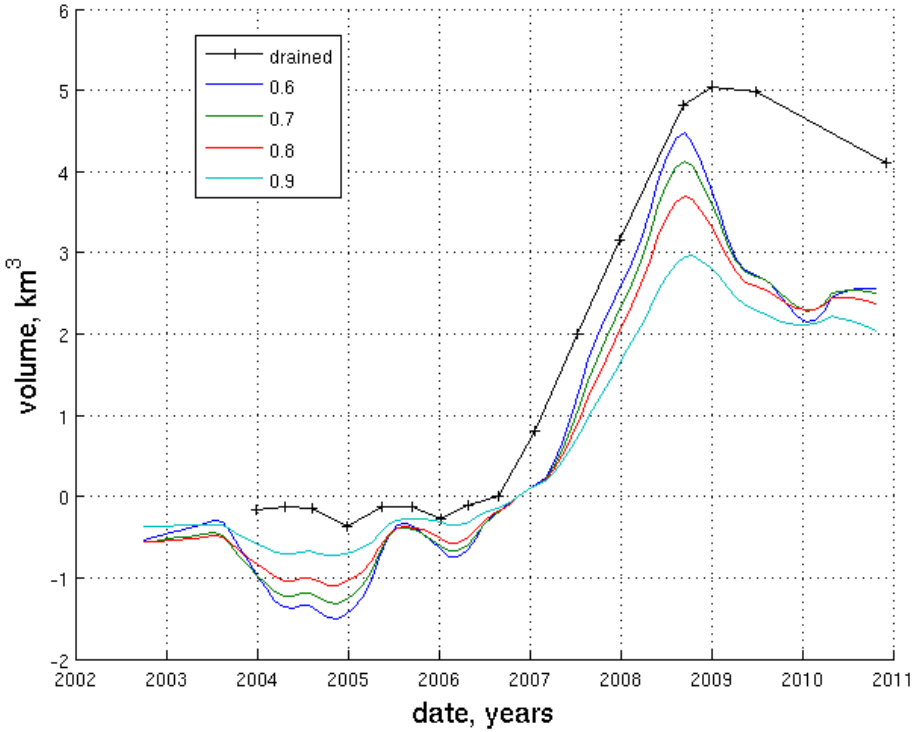

Fig. 6. Chronology of the drainage of Lake $Cook_{E2}$ and the subsequent storage/release of water in downstream lakes. Curve "drained": volume of water that drained from Lake $Cook_{E2}$, estimated from DEM differencing and ICESat measurements; other curves: volume of water stored in active lakes downstream of Lake $Cook_{E2}$, with different correlation thresholds (Sect. 4.2).

TCD
7, 841–871, 2013

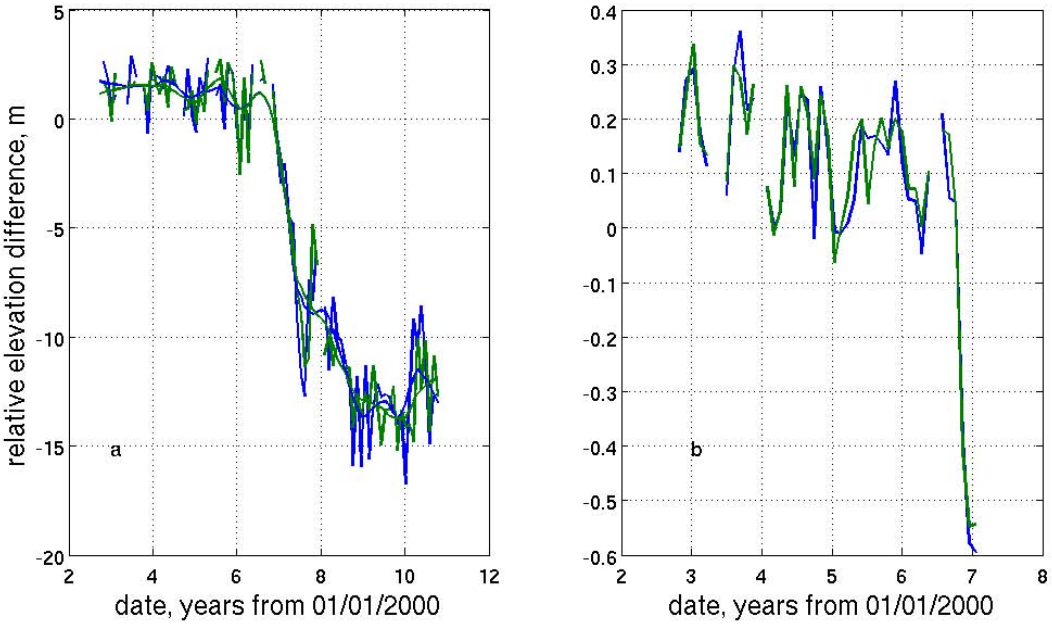

Fig. 7. (a) Relative elevation time series from Envisat radar altimetry over Lake $Cook_{E2}$. **(b)** Elevation time series computed only from the pre-drainage measurements at the same location. Note the different vertical scales.

TCD
7, 841–871, 2013

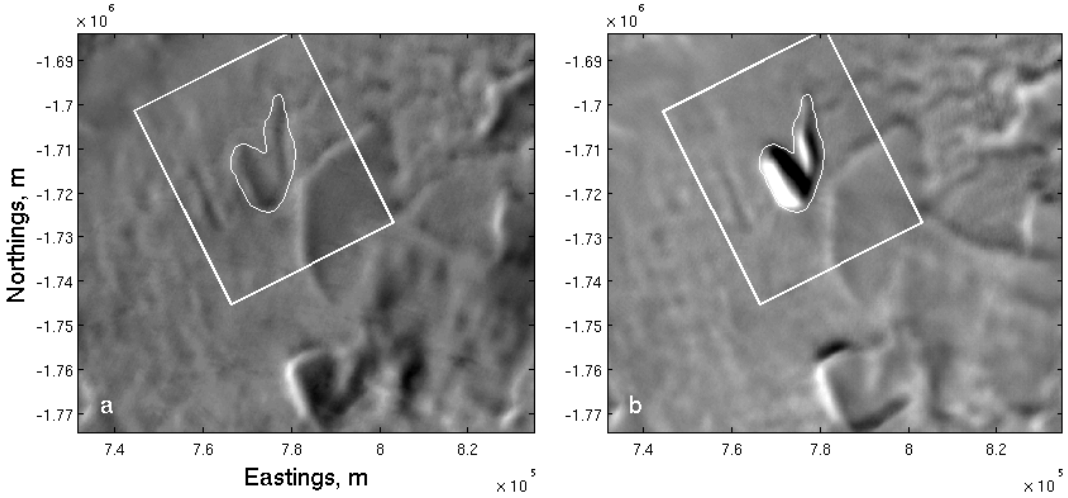

Fig. 8. Subset of the MODIS Mosaic Of Antarctica (Scambos et al., 2007) around the region of Lake $Cook_{E2}$. **(a)** 2003–2004 mosaic, **(b)** 2008–2009 mosaic processed with the same algorithm (Scambos, personal communication, 2013). This subset corresponds to the dashed line box in Fig. 3. The white box is the zone covered by Fig. 1. The white contour is the −3 m contour extracted from the map of elevation difference (Fig. 1).

TCD
7, 841–871, 2013